Johannes Kiefer, Julia Bartels, Stephen Kroll, Kurosch Rezwan

Vibrational spectroscopy as a promising toolbox for analyzing functionalized ceramic membranes

© DOI: 10.1177/0003702818769479

Vibrational Spectroscopy as a Promising Toolbox for Analyzing Functionalized Ceramic Membranes

Johannes Kiefer[1,2,3], Julia Bartels[4], Stephen Kroll[2,5], and Kurosch Rezwan[2,4]

Abstract

Ceramic materials find use in many fields including the life sciences and environmental engineering. For example, ceramic membranes have shown to be promising filters for water treatment and virus retention. The analysis of such materials, however, remains challenging. In the present study, the potential of three vibrational spectroscopic methods for characterizing functionalized ceramic membranes for water treatment is evaluated. For this purpose, Raman scattering, infrared (IR) absorption, and solvent infrared spectroscopy (SIRS) were employed. The data were analyzed with respect to spectral changes as well as using principal component analysis (PCA). The Raman spectra allow an unambiguous discrimination of the sample types. The IR spectra do not change systematically with functionalization state of the material. Solvent infrared spectroscopy allows a systematic distinction and enables studying the molecular interactions between the membrane surface and the solvent.

Keywords

Ceramic, Fourier transform infrared, FT-IR, principal component analysis, PCA, Raman, solvent infrared spectroscopy, SIRS

Date received: 15 November 2017; accepted: 15 March 2018

Introduction

Membrane-based filter technologies are widely used in chemical and environmental engineering. The main objective of a filtering process is usually to purify a fluid, e.g., drinking water, either by physical retention of particulate matter or by adsorption of atoms, ions, or molecules.[1,2] In general, the contaminants to be retained can be chemical, physical, or biological. The latter in terms of bacteria and viruses is of interest also from a societal point of view as they can have a direct influence on public health and the environment.[3,4] Therefore, cleaning water from biological contaminants such as viruses represents a particularly important task, but at the same time, it is a technological challenge. This challenge is actually twofold: first, the development of suitable membrane materials with tailored surface functionalization; and, second, the implementation of analytical methods that are capable of characterizing the materials including their surface properties.

Polymer membranes represent the state-of-the-art materials in water treatment by filtering.[5,6] However, their tendency to foul[7,8] and their reduced chemical,[9] mechanical,[10,11] and thermal[11] stability calls for suitable alternatives. Ceramic membranes can overcome the mentioned shortcomings of their polymeric counterparts.[12] Moreover, ceramic materials show no swelling behavior and hence are easier to implement and operate under constant conditions. Due to their high stability, cleaning and regeneration can be realized by (back)flushing, the application of chemicals (acidic or basic), or thermal treatment[13–16] and hence the costs for maintenance and operation are reduced. In the context of virus retention, ceramic membranes based on yttria-stabilized zirconia (YSZ) have recently shown their potential.[17–19] The ceramic capillaries were functionalized using different aminosilanes, which

[1]Technische Thermodynamik, University of Bremen, Bremen, Germany
[2]Center for Materials and Processes (MAPEX), University of Bremen, Bremen, Germany
[3]School of Engineering, University of Aberdeen, Aberdeen, UK
[4]Advanced Ceramics, University of Bremen, Bremen, Germany
[5]IfBB-Institute for Bioplastics and Biocomposites, Hochschule Hannover-University of Applied Sciences and Arts, Hannover, Germany

Corresponding author:
Johannes Kiefer, Universitaet Bremen, Badgasteiner Str 1, Bremen 28359, Germany.
Email: jkiefer@uni-bremen.de

significantly increased the virus retention performance. These materials were found to be very promising for controlled virus retention.

Analytical techniques for membranes that can be used in a straightforward manner and do not require sample preparation are highly desirable. However, the characterization of the surface chemistry and the adsorption mechanisms is often the bottleneck. It usually requires expensive equipment (e.g., electron or atomic force microscopes), sample preparation (e.g., sputtering, wet chemistry), and the application of high vacuum.[20–22] The latter immediately rejects all attempts to study a system in the presence of a volatile fluid. This problem can be overcome by optical spectroscopic methods. In particular, vibrational spectroscopic techniques are nowadays established tools and they have already found applications in the characterization of membranes. For example, attenuated total reflection Fourier transform infrared (ATR FT-IR) spectroscopy is a common tool for studying the surface chemistry of polymer membranes.[23,24] It has also been used to characterize the surface porosity[25] and to investigate protein fouling on standard and functionalized membranes.[23,26,27] Raman spectroscopy has also been applied mainly to polymer and biological membranes.[28,29] Raman applications to ceramic materials commonly utilize Fourier transform approaches [30,31] or confocal micro spectroscopy.[32,33]

The aim of this work is to develop a suitable and straightforward analytical scheme for characterizing functionalized ceramic membranes using vibrational spectroscopy. For this purpose, Raman and ATR FT-IR are applied to five membrane materials with different states of functionalization: non-functionalized YSZ; hydroxyl-activated YSZ; YSZ functionalized with 3-aminopropyltriethoxysilane (APTES); YSZ functionalized with N-(2-aminoethyl)-3-aminopropyltriethoxysilane (AE-APTES); and YSZ functionalized with N-(3-trimethoxysilylpropyl)diethylenetriamine (TPDA). A detailed description of these membrane materials and their virus retention performance can be found in Bartels et al.[19] In addition to the conventional Raman and IR techniques, the recently developed solvent infrared spectroscopy (SIRS) approach[34] is employed using water as solvent. In SIRS, the surface chemistry of a solid material is characterized in an indirect manner. The information is obtained from the vibrational spectrum of the solvent filling the cavities in a fixed bed of particles or the porous structure of the solid material.[34,35] The three methods are compared and evaluated with regard to their potential for analyzing and characterizing ceramic membranes with post-functionalizations.

Materials and Methods

Sample Preparation and Characterization

The ceramic capillary membranes made of YSZ are fabricated by extrusion and sintered at 1050 °C for 2 h in

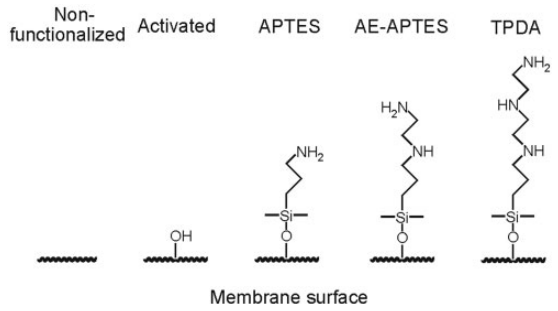

Figure 1. Schematics of the membrane surface with the functionalization states as investigated in this study (in air, non-dissociated functional groups).

accordance with our previous work to maintain a relatively high open porosity (49%) in combination with a sufficient mechanical stability (bending strength of 31 MPa) for filtration applications.[19] The zirconia powder TZ-3YS-E is stabilized with 3 mol% yttria, which corresponds to 5.2 mass%. The powder and the sintered capillaries have mainly a tetragonal structure, which was confirmed by X-ray diffraction (XRD) measurements. Activation of the membrane surface is carried out by acidic hydroxylation using Piranha solution followed by aminosilanization to tailor the loading capacity of amino groups on the membrane surface. Three model aminosilanes with one, two, or three amino groups per silane molecule are used referring to APTES, AE-APTES, and TPDA, respectively. Figure 1 shows an illustration of the different chemical surface functionalization states of the activated and amino-functionalized samples where APTES features one primary amino group, AE-APTES one primary and one secondary amino group, and TPDA one primary and two secondary amino groups. For immobilized APTES, AE-APTES, and TPDA, the total chain length consists of 6, 9, and 12 atoms, respectively. By this simplified description of the chemical surface state of amino-functionalized membranes no inter- and intramolecular crosslinking of aminosilanes is considered showing a straight orientation of single molecule chains without steric hindrance.

Based on a photometrical acid orange II assay for quantification loading capacities of 0.44 ± 0.08 (APTES), 0.51 ± 0.04 (AE-APTES), and 1.01 ± 0.09 accessible amino groups/nm^2 are determined. The results of streaming-potential measurements confirm a successful amino-functionalization and indicate positive zeta-potentials at pH 3–9 assuming isoelectric points >9, most likely in the range of $\sim$10–11. The performance of such amino-functionalized membranes is tested for virus filtration using a small model bacteriophage (MS2, $\sim$25 nm). In agreement with an increased loading capacity of amino groups on the membrane surface increased log reduction values of 5.2 ± 0.8 (APTES), 5.7 ± 0.6 (AE-APTES), and 9.6 ± 0.3 (TPDA) are obtained showing the high potential of chemical surface functionalizations for bio-engineering and environmental applications. Vibrational spectroscopy was applied

to the non-functionalized, activated (hydroxylated), and three types of aminosilanized capillary membranes (APTES, AE-APTES, TPDA).

Spectroscopy

Raman spectroscopy is the inelastic scattering of monochromatic laser light. During the scattering process, energy is transferred from the incident photon to the molecule, which undergoes a change in vibrational state. Hence, the scattered photon has a reduced energy, which gives rise to a frequency shift with respect to the incident light. Since every molecule has a unique vibrational structure, the Raman spectrum represents a molecular fingerprint. For completeness we note that in a ceramic material, like the one under study, the existence of a crystal lattice of repeating unit cells allows the propagation of vibrational waves, which are often referred to as phonons.[36] In contrast, the vibrational modes of molecules are local phenomena. The Raman spectra of the membranes were recorded using an Avantes Raman bundle with a 785 nm excitation laser and a resolution of $\sim$6 cm^{-1}. Recording ten spectra from an individual sample showed very good reproducibility. The relative intensities of the normalized spectra were virtually identical, while the absolute intensity changed by 10–15%.

Infrared (IR) spectroscopy is an absorption method in which the molecules are vibrationally excited directly by taking up a photon. The absorbed photon is removed from the radiation passing the sample, which gives rise to the absorption spectrum. Due to the different selection rules for absorption and scattering, Raman and IR spectra provide complementary information. The IR spectra of the membranes were recorded on an Agilent Cary 630 instrument equipped with a diamond unit for attenuated total reflection (ATR) spectroscopy. The spectra were acquired in the range of 650–4000 cm^{-1} with a nominal resolution of 2 cm^{-1}. The membrane samples were pressed onto the diamond crystal to obtain sufficient contact. During this procedure, the membrane geometry was destroyed. However, this is no problem, as this damage does not affect the membrane surface at the molecular level. Before the measurement, the background was taken with no sample on the ATR crystal. Thirty-two scans were averaged for each spectrum.

Solvent infrared spectroscopy spectra were recorded with the same instrument and settings described above. The relatively new concept of SIRS was described in detail in Kiefer et al.[34] In brief, a powder or porous solid is placed on the ATR crystal and fixed mechanically, usually with a metal clamp. In the second step, a droplet of a solvent is added to fill the void spaces and wet the crystal. Then, the IR spectrum is recorded and compared to that of the pure solvent. In the present work, SIRS measurements were performed with distilled water as solvent. Water was selected because the membrane materials were prepared for an application dealing with virus retention in aqueous media. We note that adding water to the membrane leads to a change in the pH value as the amino groups will be protonated.

Data Evaluation

Aside from conventional spectral analysis, the data were analyzed using principal component analysis (PCA). Principal component analysis is an unsupervised chemometric tool[37,38] that is commonly applied to spectroscopic data.[39] Principal component analysis builds a model for a data matrix X aiming at the most meaningful representation of the data set. This is obtained by reducing the dimension of the data matrix X and thereby extracting only the relevant information. The resulting principal components (PCs) represent the variance in the data set with decreasing order: the first principal component (PC1) means the largest variance, PC2 the second largest, and so on. In this context, the signal variance is a measure for the relevance of the information stored in the data set. Eventually, the PCA yields the loading matrix and the scores matrix. The scores represent the original data in the new dimensional space spanned by the PCs, whereas the loadings represent the eigenvectors and represent the contribution of the original data to creating the PC.

Results and Discussion

Raman Spectra

Figure 2a shows the raw Raman spectrum of the non-functionalized membrane. The spectrum is dominated by a broad background due to elastically scattered laser light and thus becomes increasingly intense towards the laser wavelength, which corresponds to 0 cm^{-1} in the Raman spectrum. The radiation in close vicinity to 0 cm^{-1} is blocked by an optical filter resulting in the observed dip at this position. The Raman signatures are visible on top of the background, but a clear identification and interpretation seems difficult. In order to overcome this problem, the broad background was corrected using the automatic baseline filter proposed by Turner et al.[40] The corrected spectrum is almost free of the background. The baseline corrected spectra of all membrane samples are displayed in Fig. 2b. The background itself is very similar for all samples. Since only the low-wavenumber region contains appreciable contributions, the plotted range is limited to 0–700 cm^{-1}. All spectra are very similar. The main peaks are observed at 642, 463, $\sim$323, 262, and 176 cm^{-1}. In addition, there is a shoulder band at 605 cm^{-1}. The signatures can be attributed to vibrational modes of the zirconia substrate. A detailed peak assignment can be found in the study of Bouvier and Lucazeau.[41] They studied

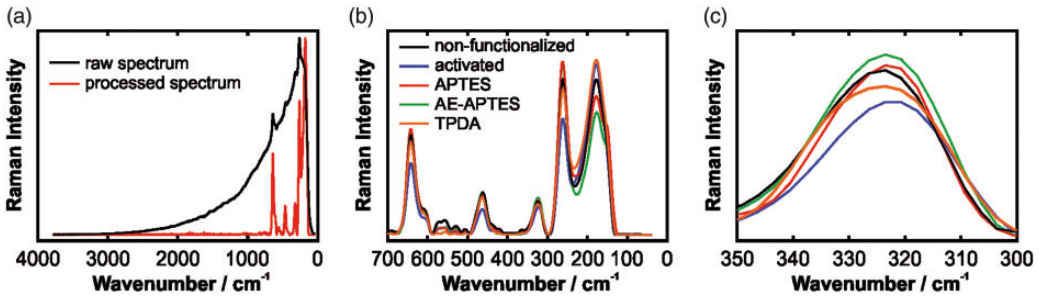

Figure 2. Raman data of the ceramic membranes: (a) raw spectrum of the non-functionalized membrane and spectrum after baseline removal; (b) processed Raman spectra of different samples; (c) zoom-in of processed spectra.

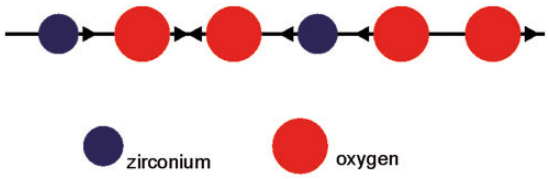

Figure 3. B_{1g} vibrational mode of zirconia illustrated schematically as linear chain model.

the pressure-dependent Raman spectrum and compared their results to the existing literature. According to their revised assignments, the observed peaks in the present work can be assigned to E_g(176 cm^{-1}), E_g(262 cm^{-1}), B_{1g}(323 cm^{-1}), E_g(461 cm^{-1}), A_{1g}(605 cm^{-1}), and B_{1g}(648 cm^{-1}) modes. Between the sample types, there are some differences in intensity. However, changes in absolute intensity are not suitable for discriminating the samples because such changes may also be caused by fluctuation in the laser intensity or alterations in the signal collection optics.

The only feature that varies in frequency and band shape for the different membrane types is the peak at around 323 cm^{-1}. This peak can be assigned to the B_{1g} vibrational mode of zirconia, which is illustrated schematically in Fig. 3. The enlarged Raman bands are displayed in Fig. 2c. Taking the spectrum of the non-functionalized membrane as reference, the peaks of the activated and amino-functionalized membranes are slightly redshifted. In addition, they change in peak intensity and shape. This is important to note, because determining such small shifts from the spectral position of the maximum amplitude only may be biased by noise and the instrument accuracy. Taking several parameters of the observed band into account provides some confidence in the shifts and their interpretation. The other peaks not shifting at all also suggests that the observation is real and not an instrumental artifact. However, it must be noted that the changes in frequency are on the order of the spectral resolution of the instrument and, hence, the effects should not be over-interpreted.

For completeness, in molecular liquids, such spectral changes can usually be attributed to changes in the strength

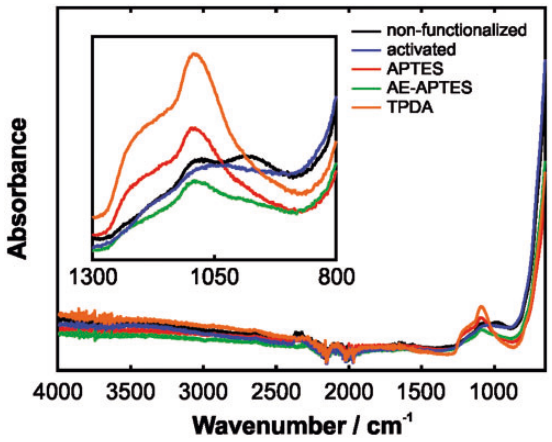

Figure 4. Raw ATR FT-IR spectra of different membrane samples. The inset shows the enlarged spectral range of 800–1300 cm^{-1} after normalization.

of covalent bonds in such a way that the strengthening of the bond results in an increase in its vibrational (stretching) frequency and vice versa for weakened bonds.[42] This model can partly be transferred in a sense that the observed redshift of the peak at 323 cm^{-1} indicates that the activation and amino-functionalization of the membrane yields a change of the bond force constants in the ceramic material. It is interesting to note that the modification of the Raman peak correlated with the number of amino groups in the silane. This becomes clearer when the spectra are plotted intensity-normalized or as difference spectra. This will be done in a comparison below.

Infrared Spectra

In the next step, the IR spectra are analyzed. The full spectral range is displayed in Fig. 4. As for the Raman spectra, the FT-IR data exhibit characteristic signals only in the fingerprint region. The most distinct differences between the different samples can be found in the range of 800–1300 cm^{-1}, shown enlarged as the inset in Fig. 4. Unfortunately, there is not a straightforward correlation with the functionalized surface chemistry. In all spectra,

the band contains three main contributions at 980, 1088, and 1200 cm^{-1}. The assignment, however, is not unambiguous as the local vibrational structure depends on the state and orientation of the zirconia polymorph.[43] Possible explanations include overtone and combination bands of strong modes occurring below 600 cm^{-1}. The shoulder around 1200 cm^{-1} may be interpreted in terms of adsorbed carbonate species.[44] However, this is unlikely due to preparation of the material. Below 800 cm^{-1}, the broad and strong background does not allow extracting useful information. The highlighted range, however, reveals clear differences in the spectral shape. This is a very interesting result from a practical point of view as the performed ATR FT-IR measurements are a straightforward and quick approach to characterize a sample. However, care must be taken when the spectra are interpreted as the ceramic material exhibits a refractive index close to that of the ATR diamond crystal.[45] Consequently, a quantitative analysis and an unambiguous vibrational assignment are difficult as the absorption features may mix with reflective signals.[46] An alternative approach would be to record IR spectra in transmission mode. The downside of this is the need for a careful sample preparation, e.g., in the form of pellets. This may introduce uncertainties as well and hence we stick to the straightforward ATR method here. For completeness, we note that a transmission IR spectrum of non-functionalized YSZ nanopowder was reported by Hajizadeh-Oghaz et al.[47] Although the spectrum was richer than our ATR FT-IR spectrum in Fig. 4, an unambiguous assignment was not given in the paper.

Solvent Infrared Spectra

The abovementioned issue of a high refractive index of the ceramic material can be overcome using the relatively new concept of SIRS. The SIRS spectrum is dominated by the solvent. Direct contributions from the solid material are small or even negligible. Solvent infrared spectroscopy allows the gaining of information about the surface chemistry of nano- and microstructured materials by analyzing the molecular interactions with an adsorbed solvent. In the present work, water was used as solvent, as the membranes are candidates for virus retention from aqueous solutions. The main interactions between the water molecules and the atoms and functional groups at the membrane surface will be hydrogen bonds. This simplifies the interpretation as the models developed for hydrogen bonding and Coulomb interactions in solutions can be employed.[42,48,49]

The OH stretching vibrational modes of water are highly sensitive to the local molecular environment and thus their band in the FT-IR spectrum will be affected by changes in the hydrogen bonding. These hydrogen-bonding interactions can take place either between water molecules or between water and the membrane surface. Figure 5 shows

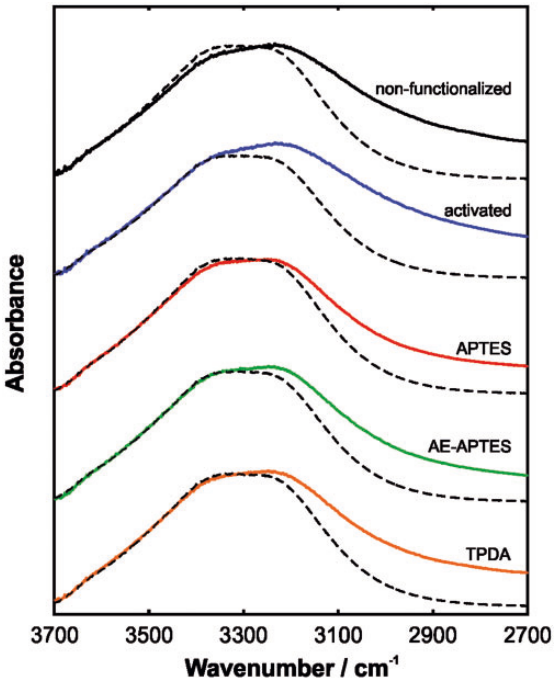

Figure 5. Solvent infrared spectra of the different membrane samples in the OH stretching region. The dashed lines represent the pure water spectrum for comparison.

the OH stretching bands of water in the vicinity of the different membrane materials. The dashed lines represent the FT-IR spectrum of pure water for comparison. The broad OH stretching band is commonly decomposed into several sub-peaks, which can be assigned to the different hydrogen bonding states of water molecules.[50,51] The high wavenumber wing results from non- or weakly hydrogen-bonded water molecules. The data in Fig. 5 clearly show that this wing (>3500 cm^{-1}) is virtually identical in all the SIRS spectra and the pure water FT-IR spectrum. This is reasonable as there will always be a small fraction of water molecules exhibiting weak intermolecular bonds and the strength of their bonds is rather independent of the molecular environment.

The highly absorbing part in the center of the OH stretching band is dominated by those water molecules that are symmetrically and anti-symmetrically hydrogen bonded to two neighboring molecules. The low-wavenumber wing represents those water molecules that are fully incorporated in tetragonal structure. As a consequence, this part of the spectrum is strongly influenced by changes in the hydrogen-bonding network. The activated sample shows the strongest deviation of the low-wavenumber wing. This can be explained by the hydroxyl groups at the activated surface, which directly affect the hydrogen-bonding network as they can act as both acceptors and donors. The SIRS spectra of the amino-functionalized membranes appear very similar at first glance. The main differences in the functional groups attached to the surface are basically

the chain length and the number of secondary amino groups (APTES: 0, AE-APTES: 1, TPDA: 2). Water molecules can interact with the amino groups and hence the changes in the shape of the OH stretching band, in particular of the low-wavenumber wing. The changes in the band shape may also be a result of a pH value change in the vicinity of the ceramic.[52] A direct contribution of the amino groups in terms of the N–H stretching vibration is not visible.

Comparison

In all three types of spectra, vibrational signatures that change with the membrane type could be identified. These features are compared in Fig. 6. The spectra have been normalized in a systematic manner in order to ease their evaluation. The Raman peak at 323 cm^{-1} changes moderately in its peak position and spectral shape, relative to the non-functionalized reference sample. The activated membrane shows the most distinct redshift (~2 cm^{-1}). The amino-functionalized membranes exhibit smaller shifts but a systematic broadening of the peak can be observed with increasing chain length (and thus with an increasing number of amino groups). These systematic variations can be seen more clearly in the difference spectra (see Fig. 6b). On both sides of the isosbestic point at ~325 cm^{-1} the spectra follow a systematic trend with increasing chain length of the amino compound and increasing number of amino groups.

No similar systematic trend can be found in the FT-IR spectra. The absorbance changes, which allows a clear distinction between the membranes. However, it does not change with chain length in the same straightforward manner as the Raman spectra. Note that the difficulties in the interpretation of FT-IR spectra of zirconia materials has been appreciated previously as well.[43] This situation changes for SIRS, where again a clear correlation with chain length is observed (Fig. 6d). The SIRS spectra have been normalized with respect to the high-wavenumber wing. This representation highlights that the water molecules, which are not or weakly involved in the hydrogen-bonding network, are hardly affected by the membrane. The low-wavenumber wing, on the other hand, allows a clear and systematic distinction. Moreover, the comparison with the reference sample indicates that the activated membrane sample leads to a stronger hydrogen-bonding network in the surrounding water, while the amino-functionalized membranes seem to lower the fraction of fully hydrogen-bonded water molecules. The distinction becomes even clearer in Fig. 6e, in which the SIRS difference spectra are plotted. The SIRS spectra were first intensity normalized with respect to the maximum absorbance in the wavenumber region of 2700–3700 cm^{-1}. In the second step, the analogously normalized spectrum of pure water was subtracted. Difference spectra exhibit an

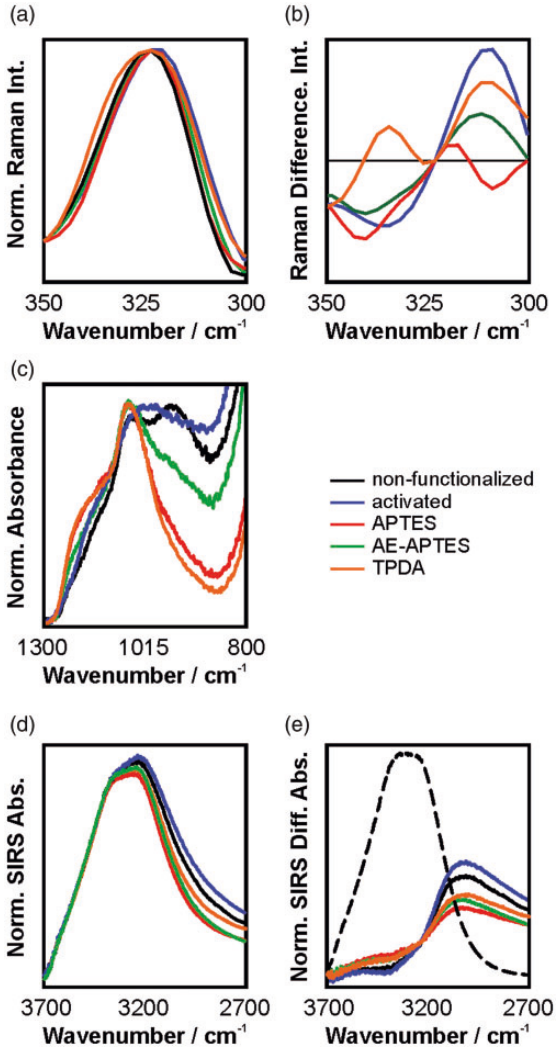

Figure 6. Normalized spectral features to allow distinction of different membrane surface functionalization states: (a) Raman spectrum; (b) Raman difference spectrum; (c) FT-IR spectrum; (d) SIRS spectrum; and (e) SIRS difference spectrum after normalization. The dashed line in (e) represents the FT-IR spectrum of pure water for comparison.

isobestic point at 3233 cm^{-1}. Interestingly, this point perfectly coincides with the position of a sub-profile that can be determined by fitting the overall OH-stretching band of water to a sum of Gaussian profiles, see Wallace et al.[50] and Kiefer et al.[53] and the discussion above. The ~3230 cm^{-1} mode can be assigned to symmetrically hydrogen-bonded water. As aforementioned, the difference spectra suggest that the fraction of strongly hydrogen-bonded water molecules increases. This increase is particularly pronounced for the activated and slightly less for the non-activated ceramic material. The three functionalized samples are close to each other but clearly show a trend with the number of NH groups: the more NH groups the stronger the influence on the hydrogen-bonding network.

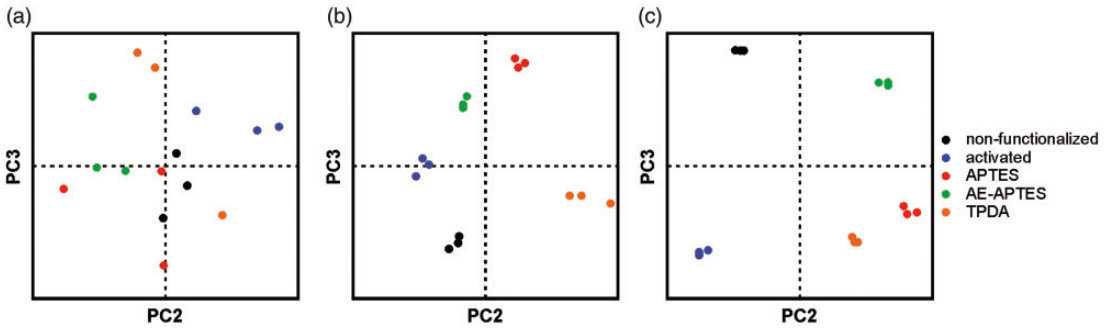

Figure 7. Principal component analysis results of the raw data. PC3 vs. PC2 for (a) Raman spectra, (b) FT-IR spectra, and (c) SIRS spectra.

The above analyses of the spectra have shown that all three methods allow the distinction between the samples when looking at characteristic features. However, it must be admitted that some of these features are not prominent at first glance. Hence, an unexperienced person may be unable to make use of the data. In order to check whether or not the spectra can be assigned to the corresponding materials, PCA was applied to the raw data. Principal component analysis is a statistical procedure that makes an orthogonal transformation to convert a set of observations of possibly correlated variables into a set of values of linearly uncorrelated variables.[38,54,55] The uncorrelated variables are the PCs. In other words, the PCA searches for characteristic signatures in the spectra.

In all three types of spectra, the first PC, PC1, is dominated by the background or pure solvent contributions. Hence, we focus on PC2 and PC3. Interestingly, in the PCA results of the SIRS spectra (note that the plots of the scores vs. wavenumber are not shown), PC2 seems dominated by water molecules that are weakly hydrogen-bonded while PC3 represents the strongly hydrogen-bonded species. For the other data sets, such a clear assignment of the PCs was not possible. Plotting PC3 against PC2 for all three methods yields the graphs in Fig. 7. For the Raman spectra, the data representing the individual materials do not lie close to each other. This means a poor classification of the data. In other words, the unprocessed full-range Raman spectra are not suitable for identifying the ceramic materials unambiguously. This can be attributed to the strong background from elastically scattered light. We note that removing the background beforehand and limiting the spectral window to the fingerprint region from 100 to 700 cm^{-1} yielded a reasonably good classification; however, this procedure can no longer be called "unsupervised". In contrast, the FT-IR and SIRS spectra allow a clear classification without pre-processing of the data. Judging from the available three measurements of each material, the SIRS data points in Fig. 7c are even a bit closer together than those in Fig. 7b. This highlights the good reproducibility of SIRS.

Conclusion

In this study, we have demonstrated the use of vibrational spectroscopy for distinguishing and characterizing functionalized ceramic membranes. For this purpose, Raman, ATR FT-IR, and SIRS were applied to amino-functionalized yttria-stabilized zirconia membranes. A non-functionalized and an activated YSZ membrane were used as references. All three methods are capable of discriminating between the different chemical surface functionalities. Raman and SIRS turned out to be particularly useful as they contain spectral features, which correlate with the chain length and number of amino groups based on used aminosilane. All three methods were applied without any specific means of sample preparation in order to test the potential of the techniques for rapid screening and deployment in the field. This is especially promising as Raman and IR methods currently experience a push towards hand-held and portable instrumentation.[56,57] Furthermore, combined vibrational spectroscopy methods can open up the door for a straightforward analysis of chemical surface functionalities independent from the starting material being of ceramic, polymer, or metal origin. Moreover, the vibrational techniques under study cannot only be applied to membranes but also to functionalized colloidal particles that are common in protein adsorption.[58]

However, Raman spectroscopy was found to strongly suffer from elastically scattered light. The resulting background led to difficulties in the data analysis and interpretation. In fact, data classification via PCA yielded poor results when the raw data were used. In contrast, the raw FT-IR and SIRS spectra provided a very good classification through PCA. Consequently, the Raman method may pose a challenge, in particular when ceramic materials are analyzed by unexperienced personnel. Fourier transform IR and SIRS seem better suited in this regard.

Solvent infrared spectroscopy was identified as a particularly interesting approach as it enables the investigation of adsorption effects. This includes the evaluation of how the membrane surface influences the molecular behavior of a

solvent. In this study, water was used as solvent and the SIRS spectra revealed systematic changes in the hydrogen-bonding network, depending on the functionalization of the ceramic material. Therefore, the SIRS approach may offer an opportunity to gain a bigger picture of the adsorption mechanisms of molecules and bioactive systems like viruses at ceramic membranes. The membranes under investigation have previously shown their potential for controlled virus retention from aqueous media. Hence, SIRS may allow accessing the interfacial mechanisms between a virus loaded surface of a membrane and a water flow. This is the subject of ongoing work in our labs. Further interesting points will be the investigation of effects due to temperature and pH variations as both are known to manifest as changes in the hydrogen-bonding network. Moreover, the application of nonlinear optical techniques[59] will enable the extension of the vibrational toolbox for ceramic membrane characterization.

Acknowledgments

The authors thank Avantes BV (Apeldoorn, The Netherlands) for the loan of the Raman instrument.

Conflict of Interest

The authors report there are no conflicts of interest.

Funding

This work was partially supported by German Research Foundation (DFG) within the Research Training Group GRK 1860 "Micro-, meso- and macroporous nonmetallic Materials: Fundamentals and Applications" (MIMENIMA).

ORCID iD

Johannes Kiefer http://orcid.org/0000-0002-0837-3456

References

1. J.M. Dickhout, Y. Moreno, P.M. Biesheuvel, L. Boels, et al. "Produced Water Treatment by Membranes: A Review from a Colloidal Perspective". J. Colloid Interface Sci. 2017. 487: 523–534.
2. S.L. Loo, A.G. Fane, W.B. Krantz, T.T. Lim. "Emergency Water Supply: A Review of Potential Technologies and Selection Criteria". Water Res. 2012. 46(10): 3125–3151.
3. A. Gadgil. "Drinking Water in Developing Countries". Annu. Rev. Energ. Environ. 1998. 23(1): 253–286.
4. J.T. Dongdem, I. Soyiri, A. Ocloo. "Public Health Significance of Viral Contamination of Drinking Water". Afr. J. Microbiol. Res. 2009. 3(12): 856–861.
5. A.M. ElHadidy, S. Peldszus, M.I. Van Dyke. "An Evaluation of Virus Removal Mechanisms by Ultrafiltration Membranes Using MS2 and ϕx174 Bacteriophage". Separ. Purif. Technol. 2013. 120: 215–223.
6. J. Langlet, L. Ogorzaly, J.C. Schrotter, C. Machinal, et al. "Efficiency of MS2 Phage an Qb Phage Remova by Membrane Filtration in Water Treatment: Applicability Ofreal-Time RT-PCR Method". J. Membr. Sci. 2009. 326(1): 111–116.
7. V.M. Kochkodan, V.K. Sharma. "Graft Polymerization and Plasma Treatment of Polymer Membranes for Fouling Reduction: A Review". Journal of Environmental Science and Health – Part A: Toxic/Hazardous Substances & Environmental Engineering. 2012. 47(12): 1713–1727.
8. A.V.R. Reddy, D.J. Mohan, A. Bhattacharya, V.J. Shah, et al. "Surface Modification of Ultrafiltration Membranes by Preadsorption of a Negatively Charged Polymer I. Permeation of Water Soluble Polymers and Inorganic Salt Solutions and Fouling Resistance Properties". J. Membr. Sci. 2003. 214(2): 211–221.
9. E. Arkhangelsky, D. Kuzmenko, N.V. Gitis, M. Vinogradov, et al. "Hypochlorite Cleaning Causes Degradation of Polymer Membranes". Tribology Letters. 2007. 28(2): 109–116.
10. J. Kiefer, G. Wei, L. Colombi Ciacchi, E. Von Lieres. "Irreversible Damage of Polymer Membranes During Attenuated Total Reflection Infrared Analysis". Appl. Spectrosc. 2017. 71(6): 1127–1133.
11. G.D. Vilakati, E.M.V. Hoek, B.B. Mamba. "Probing the Mechanical and Thermal Properties of Polysulfone Membranes Modified with Synthetic and Natural Polymer Additives". Polymer Test. 2014. 34: 202–210.
12. A. Muric, I. Petrinic, M.L. Christensen. "Comparison of Ceramic and Polymeric Ultrafiltration Membranes for Treating Wastewater from Metalworking Industry". Chem. Eng. J. 2014. 255: 403–410.
13. P. Blanpain-Avet, J.F. Migdal, T. Benezech. "Chemical Cleaning of a Tubular Ceramic Microfiltration Membrane Fouled with a Whey Protein Concentrate Suspension-Characterization of Hydraulic and Chemical Cleanliness". J. Membr. Sci. 2009. 337(1–2): 153–174.
14. T. Quadt, E. Schmidt. "Membranes: Optimising the Regeneration of Ceramic Membranes". Filtrat. Separ. 2011. 48(6): 26–28.
15. H. Fadaei, S.R. Tabaei, R. Roostaazad. "Comparative Assessment of the Efficiencies of Gas Sparging and Back-Flushing to Improve Yeast Microfiltration Using Tubular Ceramic Membranes". Desalination. 2007. 217(1–3): 93–99.
16. E.P. Garmash, Y.N. Kryuchkov, V.N. Pavlikov. "Ceramic Membranes for Ultra- and Microfiltration". Glass Ceram. 1995. 52(5–6): 150–152.
17. S. Kroll, M.O.C. de Moura, F. Meder, G. Grathwohl, et al. "High Virus Retention Mediated by Zirconia Microtubes with Tailored Porosity". J. Eur. Ceram. Soc. 2012. 32(16): 4111–4120.
18. J. Werner, B. Besser, S. Kroll, K. Rezwan. "Production of Ceramic Membranes with Different Pore Sizes for Virus Retention". Journal of Water Process Engineering. 2014. 4: 201–211.
19. J. Bartels, M.N. Souza, A. Schaper, P. Arki, et al. "Amino-Functionalized Ceramic Capillary Membranes for Controlled Virus Retention". Env. Sci. Technol. 2016. 50(4): 1973–1981.
20. E. Mirtalebi, M.M.A. Shirazi, A. Kargari, M. Tabatabaei, et al. "Assessment of Atomic Force and Scanning Electron Microscopes for Characterization of Commercial and Electrospun Nylon Membranes for Coke Removal from Wastewater". Desalination and Water Treatment. 2014. 52(34–36): 6611–6619.
21. K.C. Khulbe, T. Matsuura, C.Y. Feng, G. Lamarche. "Characterization of Ultrafiltration Membrane Prepared from Poly Ethersulfone by Using Electron Spin Resonance Technique". Separ. Purif. Technol. 2002. 29(1): 15–22.
22. B. Das, B. Chakrabarty, P. Barkakati. "Preparation and Characterization of Novel Ceramic Membranes for Micro-Filtration Applications". Ceram. Int. 2016. 42(13): 14326–14333.
23. S. Belfer, R. Fainchtain, Y. Purinson, O. Kedem. "Surface Characterization by FTIR-ATR Spectroscopy of Polyethersulfone Membranes - Unmodified, Modified and Protein Fouled". J. Membr. Sci. 2000. 172: 113–124.
24. M.R. Pereira, J. Yarwood. "ATR-FTIR Spectroscopic Studies of the Structure and Permeability of Sulfonated Poly(Ether Sulfone) Membranes .1. Interfacial Water-Polymer Interactions". J. Chem. Soc. Faraday Trans. 1996. 92(15): 2731–2735.
25. J. Kiefer, N.H. Rasul, P.K. Ghosh, E. Von Lieres. "Surface and Bulk Porosity Mapping of Polymer Membranes Using Infrared Spectroscopy". J. Membr. Sci. 2014. 452: 152–156.
26. T. Maruyama, S. Katoh, M. Nakajima, H. Nabetani, et al. "FT-IR Analysis of Bsa Fouled on Ultrafiltration and Microfiltration Membranes". J. Membr. Sci. 2001. 192(1–2): 201–207.

27. G.D. Kang, Z.N. Liu, H.J. Yu, Y.M. Cao. "Enhancing Antifouling Property of Commercial Polyamide Reverse Osmosis Membrane by Surface Coating Using a Brush-Like Polymer Containing Poly (Ethylene Glycol) Chains". Desalination and Water Treatment. 2012. 37(1–3): 139–145.
28. M. Hara, J. Inukai, B. Bae, T. Hoshi, et al. "Micro-Raman Study on Water Distribution inside a Nafion Membrane During Operation of Polymer Electrolyte Fuel Cell". Electrochim. Acta. 2012. 82: 277–283.
29. R.A. Dluhy, S.M. Stephens, S. Widayati, A.D. Williams. "Vibrational Spectroscopy of Biophysical Monolayers - Applications of IR and Raman Spectroscopy to Biomembrane Model Systems at Interfaces". Spectrochim. Acta A. 1995. 51(8): 1413–1447.
30. M.T. Colomer, C. Guglieri, S. Diaz-Moreno, M. Maczka, et al. "Effect of Titania Doping and Sintering Temperature on Titanium Local Environment and Electrical Conductivity of YSZ". J. Alloy. Comp. 2016. 689: 512–524.
31. S.G. Rathod, R.F. Bhajantri, V. Ravindrachary, T. Sheela, et al. "Pressure Sensitive Dielectric Properties of TiO2 Doped PVA/CN-Li Nanocomposite". J. Polymer Res. 2015. 22(2): 6.
32. M. Romero, R. Faccio, S. Vazquez, S. Davyt, et al. "Experimental and Theoretical Raman Study on the Structure and Microstructure of Li0.30la0.57TiO3 Electrolyte Prepared by the Sol-Gel Method in Acetic Medium". Ceram. Int. 2016. 42(14): 15414–15422.
33. O.A. Maslova, G. Guimbretiere, M.R. Ammar, L. Desgranges, et al. "Raman Imaging and Principal Component Analysis-Based Data Processing on Uranium Oxide Ceramics". Mater. Char. 2017. 129: 260–269.
34. J. Kiefer, J. Grabow, H.-D. Kurland, F.A. Müller. "Characterization of Nanoparticles by Solvent Infrared Spectroscopy". Anal. Chem. 2015. 87(24): 12313–12317.
35. M.P. Singh, N.R. Dhumal, H.J. Kim, J. Kiefer, et al. "Influence of Water on the Chemistry and Structure of the Metal-Organic Framework Cu3(BTC)2". J. Phys. Chem. C. 2016. 120(31): 17323–17333.
36. D. Tuschel. "Why Are the Raman Spectra of Crystalline and Amorphous Solids Different?" Spectroscopy. 2017. 32(3): 26–33.
37. H.H. Nieuwoudt, B.A. Prior, I.S. Pretorius, M. Manley, et al. "Principal Component Analysis Applied to Fourier Transform Infrared Spectroscopy for the Design of Calibration Sets for Glycerol Prediction Models in Wine and for the Detection and Classification of Outlier Samples". J. Agric. Food Chem. 2004. 52(12): 3726–3735.
38. S. Wold, K. Esbensen, P. Geladi. "Principal Component Analysis". Chemometr. Intell. Lab. Syst. 1987. 2(1–3): 37–52.
39. J. Kiefer, K. Eisen. "Unsupervised Screening of Vibrational Spectra by Principal Component Analysis for Identifying Molecular Clusters". ChemPhysChem. 2018. 19(7): 795–800.
40. H.G. Schulze, R.B. Foist, K. Okuda, A. Ivanov, et al. "A Model-Free, Fully Automated Baseline-Removal Method for Raman Spectra". Appl. Spectrosc. 2011. 65(1): 75–84.
41. P. Bouvier, G. Lucateau. "Raman Spectra and Vibrational Analysis of Nanometric Tetragonal Zirconia under High Pressure". J. Phys. Chem. Solid. 2000. 61(4): 569–578.
42. J. Joseph, E.D. Jemmis. "Red-, Blue-, or No-Shift in Hydrogen Bonds: A Unified Explanation". J. Am. Chem. Soc. 2007. 129(15): 4620–4632.
43. E. Fernandez Lopez, V. Sanchez Escribano, M. Panizza, M.M. Carnasciali, et al. "Vibrational and Electronic Spectroscopic Properties of Zirconia Powders". J. Mater. Chem. 2001. 11(7): 1891–1897.
44. E.M. Köck, M. Kogler, T. Bielz, B. Klötzer, et al. "In Situ FT-IR Study of CO2 and CO Adsorption on Y2O3, ZrO2, and Yttria-Stabilized ZrO2". J. Phys. Chem. C. 2013. 117(34): 17666–17673.
45. D.L. Wood, K. Nassau, T.Y. Kometani. "Refractive Index of Y2O3 Stabilized Cubic Zirconia: Variation with Composition and Wavelength". Appl. Opt. 1990. 29(16): 2485–2488.
46. M. Miljkovic, B. Bird, M. Diem. "Line Shape Distortion Effects in Infrared Spectroscopy". Analyst. 2012. 137(17): 3954–3964.
47. M. Hajizadeh-Oghaz, R.S. Razavi, M.R. Loghman-Estarki. "Synthesis and Characterization of Non-Transformable Tetragonal YSZ Nanopowder by Means of Pechini Method for Thermal Barrier Coatings (TBCs) Applications". Journal of Sol-Gel Science and Technology. 2014. 70(1): 6–13.
48. J. Kiefer, M. Molina Martinez, K. Noack. "The Peculiar Nature of Molecular Interactions between an Imidazolium Ionic Liquid and Acetone". ChemPhysChem. 2012. 13(5): 1213–1220.
49. K. Noack, J. Kiefer, A. Leipertz. "Concentration Dependent Hydrogen Bonding Effects on the Dimethyl Sulfoxide Vibrational Structure in the Presence of Water, Methanol and Ethanol". ChemPhysChem. 2010. 11(3): 630–637.
50. V.M. Wallace, N.R. Dhumal, F.M. Zehentbauer, H.J. Kim, et al. "Revisiting the Aqueous Solutions of Dimethyl Sulfoxide by Spectroscopy in the Mid- and near-Infrared: Experiments and Car-Parrinello Simulations". J. Phys. Chem. B. 2015. 119(46): 14780–14789.
51. D.A. Schmidt, K. Miki. "Structural Correlations in Liquid Water: A New Interpretation of IR Spectroscopy". J. Phys. Chem. A. 2007. 111(40): 10119–10122.
52. J.J. Max, C. Chapados. "Subtraction of the Water Spectra from Infrared Spectra of Acidic and Alkaline Solutions". Appl. Spectrosc. 1998. 52(7): 963–969.
53. J. Kiefer, K. Frank, F.M. Zehentbauer, H.P. Schuchmann. "Infrared Spectroscopy of Bilberry Extract Water-in-Oil Emulsions: Sensing the Water-Oil Interface". Biosensors. 2016. 6(2): 13.
54. H. Hotelling. "Analysis of a Complex of Statistical Variables into Principal Components". J. Educ. Psychol. 1933. 24(6): 417.
55. K. Pearson. "Principal Components Analysis". The London, Edinburgh, and Dublin Philosophical Magazine and Journal of Science. 1901. 6(2): 559.
56. J. Jehlička, A. Culka, D. Bersani, P. Vandenabeele. "Comparison of Seven Portable Raman Spectrometers: Beryl as a Case Study". J. Raman Spectrosc. 2017. 48(10): 1289–1299.
57. C. Koch, A.E. Posch, C. Herwig, B. Lendl. "Comparison of Fiber Optic and Conduit Attenuated Total Reflection (ATR) Fourier Transform Infrared (FT-IR) Setup for In-Line Fermentation Monitoring". Appl. Spectrosc. 2016. 70(12): 1965–1973.
58. F. Meder, H. Hintz, Y. Koehler, M.M. Schmidt, et al. "Adsorption and Orientation of the Physiological Extracellular Peptide Glutathione Disulfide on Surface Functionalized Colloidal Alumina Particles". J. Am. Chem. Soc. 2013. 135(16): 6307–6316.
59. J. Kiefer, A. Materny, J. Moger, H.L. Offerhaus, et al. "Advances in Nonlinear Optical Spectroscopies: A Historical Perspective of Developments and Applications Presented at ECONOS". J. Raman Spectrosc. 2016. 47(9): 1111–1123.